Journal of Nuclear Materials 400 (2010) 240–244

Contents lists available at ScienceDirect

Journal of Nuclear Materials

journal homepage: www.elsevier.com/locate/jnucmat

# A new Fe–He pair potential

N. Gao [a], M. Samaras [a], H. Van Swygenhoven [b,*]

[a] NES – High Temperature Materials, Paul Scherrer Institute, CH-5232 Villigen PSI, Switzerland
[b] NUM/ASQ – Materials Science and Simulation, Paul Scherrer Institute, CH-5232 Villigen PSI, Switzerland

ARTICLE INFO

*Article history:*
Received 11 December 2009
Accepted 16 March 2010

ABSTRACT

A pair potential for the Fe–He system has been developed based on recent magnetic potentials of Fe and *ab initio* data. The new potentials can reproduce simple He defects, the migration energy of the tetrahedral He interstitial and various He cluster properties in single crystal system of bcc iron with He atoms. The potentials are used to study the He energetics of single and bi-interstitial clusters in a $\Sigma 3(1\,1\,2)$ boundary plane using a bi-crystal simulation geometry.



## 1. Introduction

Helium atoms generated during the irradiation process have been suggested to be one of the main reasons for the degradation of materials used in nuclear energy reactor systems. The accumulation of helium atoms in materials can induce bubble formation, void swelling, changes in microstructure, high temperature embrittlement and blistering [1–4]. Ferritic steels are proposed to be the structural materials in future fission and fusion reactors. Steels used in fusion reactor will be subject to high energy neutron irradiation which will produce helium through $(n, \alpha)$ transmutations. Therefore, to understand the behavior of helium in bcc iron becomes a crucial issue in the research of usable structural reactor materials. In an experimental study, information about the radiation damage process, especially the early stages, is not easily accessible due to the extremely short timescales at which they occur. Molecular dynamics (MD) and Monte Carlo (MC) simulations have been used to try to understand the behavior of He in reactor materials, such as the cascade studies to determine the primary damage state in Fe and subsequent defect evolution [5]. However, the results of MD for the Fe–He and alloy systems are found to depend on the choice of the pure Fe empirical potential model and the Fe–He cross potential. A Helium atom can strongly bind with a vacancy, a helium-vacancy cluster or other defects, such as a dislocation or a grain boundary, which will affect the process of irradiation. In early work, most simulations for He in Fe were based on the Johnson and Wilson Fe–He potential [6], which predicted that the octahedral interstitial He is the ground state interstitial structure [7]. However recent DFT calculations have demonstrated that it is the tetrahedral He interstitial structure that has the lowest energy [8]. An EAM potential for Fe–He using a three-body Fe–He interaction has also been developed [9], in which it was argued that such an angular dependent term was needed to fit to the available *ab initio* helium defect energy data [9] – despite He being a closed shell Nobel gas atom. A disadvantage of such a construction is that the three-body potential requires more computational time than a simple pair potential.

On the other hand, Juslin and Nordlund have demonstrated that a pair potential is sufficient to reproduce the properties of single He in bulk bcc iron [10]. In the process of fitting suggested by Juslin and Nordlund, only the properties of single He in bcc iron were used. These include the substitutional, octahedral and tetrahedral He formation energies [10]. The properties of complex He-defect clusters were not used. In high temperature, this potential shows no clustering of He in bcc iron [11]. Moreover, in both of these approaches, an EAM potential with three-body term and pair potential, have been fitted using non-magnetic Fe empirical potential models. It has however been demonstrated by DFT that ferromagnetism plays an important role in bcc Fe [12] and therefore a number of new potentials have been developed based on the so-called "magnetic potential" formalism [13]. In this paper, the approach of Juslin and Nordlund is followed however more flexible knot functions are used to describe the interaction of Fe–He, and two new Fe–He pair potentials are presented that are optimized within the magnetic potential formalism for bcc Fe [13,14]. Additionally, several He-cluster binding energies are also included in the fitting. In order to reproduce the diffusion properties of free He atoms, the migration energy of single He interstitial defects is also included in the fitting process, which means that the saddle point of an intermediate energy barrier of the Fe–He system is employed. The interaction between He is described by the traditional potential of Beck [15]. It is found that the new pair potentials can reproduce simple He defects, the migration energy of the tetrahedral He interstitial and various He cluster properties in single crystal system of bcc iron with He atoms. The potentials are also used to

* Corresponding author. Tel.: +41 56 310 2931; fax: +41 56 310 3131.
*E-mail address:* helena.vs@psi.ch (H. Van Swygenhoven).

0022-3115/$ - see front matter © 2010 Elsevier B.V. All rights reserved.
doi:10.1016/j.jnucmat.2010.03.009

study the He energetics of single and bi-interstitial clusters in a Σ3(1 1 2) boundary plane using a bi-crystal simulation geometry.

## 2. *Ab initio* Fe–He data and fitting methodology

Juslin and Nordlund have suggested [10] that *ab initio* data calculated for the Fe–He dimer with Dmol97 [16,17] can be used to describe the short range interaction between Fe and He. This dimer data is important for short range interactions at high energies but not appropriate to describe the long distance interaction between Fe and He responsible for material cohesion. This data will also be used presently. In addition DFT data for small He defects in Fe exists. This has been calculated mainly by two groups, Seletskaia et al. [9,18] using the VASP code and Fu and Willaime [8,19] using the SIESTA code. This data is listed in Table 1. Inspection of this table demonstrates that there is not complete agreement amongst the DFT calculations, in particular the binding energy for the $He_2$ cluster calculated by VASP [9] is 0 eV whereas for the SIESTA[19] calculation it is 0.43 eV. In the present work the data calculated using SIESTA is employed. The formation energy of a $He_nV_m$ cluster is defined as following:

$$E_f(\mathrm{He}_n\mathrm{V}_m) = E_{\mathrm{tot}}(\mathrm{He}_n\mathrm{V}_m) - [nE_{\mathrm{He}} + (N-m)E_{\mathrm{Fe}}] \quad (1)$$

where $N$ is total number of Fe atoms; $E_{\mathrm{He}}$ and $E_{\mathrm{Fe}}$ are cohesive energy of perfect fcc He crystal and bcc Fe crystal, respectively. For different bcc Fe potentials, different $E_{\mathrm{Fe}}$s are used. $E_{\mathrm{He}}$ is calculated to be −0.0078 eV/atom which is close to both −0.0080 eV/atom [20] and −0.00714 eV/atom used by Morishita et al. [21]. The binding energy of a single He to $He_nV_m$ cluster can then be calculated with the formation energy of single He, $He_nV_m$ and $He_{n+1}V_m$ cluster:

$$E_b(\mathrm{He}) = E_f(\mathrm{He}) + E_f(\mathrm{He}_n\mathrm{V}_m) - E_f(\mathrm{He}_{n+1}\mathrm{V}_m) \quad (2)$$

where $E_f$(He) is the formation energy of He at tetrahedral interstitial site and $E_f(\mathrm{He}_i\mathrm{V}_j)$ is formation energy of He–V cluster and calculated with Eq. (1).

Juslin and Nordlund [10] considered the repulsive nature of helium in iron as a screened Coulomb potential, that is, $f(r) = (a + b/r)\exp(-cr)$. In the present work a 5th order knot function representation is instead used for added flexibility. Knot functions have been used successfully to describe the interactions of Fe–Fe [13,14] and Fe–C [22]. In the short range regime of the Fe–He interaction, the *ab initio* dimer data is also used to a range of $R_1$ which is a little shorter than that used in Ref. [10]. From $R_1$ to $R_2$ a spline representation is used, and in the regime greater than $R_2$ the aforementioned knot functions are employed. The spline representation to extrapolate between the dimer data and the present empirical Fe–He knot function representation was optimized to ensure continuity up to the second order derivative. The potential therefore has the following form:

$$f(r) = \begin{cases} \text{Dmol-potential} & r \le R_1 \\ \text{Spline-data} & R_1 \le r \le R_2 \\ \sum_{i=1}^{N} a_i (r_i - r)^5 \theta(r_i - r) & r \geqslant R_2 \end{cases} \quad (3)$$

where $R_1$ and $R_2$ are short range cutoff distances defined above. Here $N$ is the number of knot functions used and $\Theta(x)$ is a Heaviside step function defined as $\Theta(x) = 1$ for $x > 0$ and $\Theta(x) = 0$ for $x < 0$. The knot coefficients $a_i$ are the parameters to be optimized in order to reproduce a variety of physical properties, whereas the knot positions $r_i$ are fixed.

In the present fitting, the defect formation energies of relaxed substitutional, octahedral, tetrahedral He interstitials, and the binding energies of $He_2$ and $He_3$ clusters are used as well as the migration energy of the tetrahedral He interstitial. These energies are calculated with the method suggested above. The SIESTA [8,19] values presently used are listed in Table 1. To obtain the relaxed defect structures for a given candidate potential, the molecular statics method is used with a periodic cell size of $4 \times 4 \times 4a_0$ in which the appropriate number of He atoms are added either substitutionally or interstitially. Volume (hydrostatic pressure) relaxation is also employed in order to compare directly with the *ab initio* results [8,19]. After relaxation, defect formation energies, binding energies and migration energy have been calculated to compare with *ab initio* values. Within the fitting program, the Nudged Elastic Band (NEB) method [23] is used to determine the migration energy for the ground state tetrahedral He interstitial. The NEB method can easily find the saddle point of the system between two known lower energy states by optimizing the chain of images of the system. By finding the saddle point the important migration energy can therefore be found. The details of this method can be found in [23]. The shape of each minimum energy pathway calculated with NEB is also checked. Only the parabola with maximal value is selected to calculate the migration energy. During the calculation of migration energy, the optimization was performed under constant volume conditions since volume relaxation was found to have negligible effect on the migration barrier. The actual fitting was performed by using a combination of simulated annealing and non-linear simplex methods.

## 3. Results

Two Fe–He potentials are fitted using different Fe magnetic potentials. The first one is the Dudarev and Derlet potential [13] and the second one is a recently developed parameterization of the magnetic potential by Chiesa et al. [14] – in particular CS3–30 (see Ref. [14]). In the current work, FeHepot1 and FeHepot2 are the Fe–He potentials for these respective magnetic potentials. The fitted parameters are listed in Table 2. The spline data used from $R_1$ to $R_2$ is listed in Table 3 for FeHepot1 and FeHepot2. For

**Table 1**
Formation and binding energies of helium defects in bcc iron. All values are in eV. The defect formation energy or binding energy are: $E^f$sub = substitutional He formation energy, $E^f$oct = octahedral He formation energy, $E^f$tet = tetrahedral He formation energy, $E^b\mathrm{He}_2$ = binding energy of He to He and $E^b\mathrm{He}_3$ = binding energy of He to $He_2$ cluster. The Fe–Fe interactions are: FS = Finnis–Sinclair, AMS = Ackland–Mendelev, DUD = Dudarev–Derlet and CDD = Chiesa–Derlet–Dudarev.

| | | Fe–Fe | $E^f$sub | $E^f$oct | $E^f$tet | $E^b\mathrm{He}_2$ | $E^b\mathrm{He}_3$ | Em |
|---|---|---|---|---|---|---|---|---|
| DFT | Seletskaia et al. [9,18] Fu and Willaime[8,19] | | 4.08(3.73[a]) | 4.60 | 4.36 | 0.00 | | |
| | | | 4.22 | 4.57 | 4.39 | 0.43 | 0.95 | 0.06 |
| MD | Seletskaia et al. [9] | FS | 3.82 | 4.74 | 4.37 | 0.15 | | |
| | Juslin and Nordlund [10] | AMS | 4.10 | 4.51 | 4.39 | −0.01 | 0.34 | 0.07 |
| | | DUD | 4.21 | 4.44 | 4.33 | −0.01 | 0.32 | 0.067 |
| | | FS | 4.12 | 4.41 | 4.29 | | | |
| | This work: FeHepot1 | DUD | 4.22 | 4.52 | 4.41 | 0.25 | 0.38 | 0.063 |
| | FeHepot2 | CDD | 4.22 | 4.58 | 4.44 | 0.20 | 0.56 | 0.063 |

[a] The value has been adjusted by Seletskaia et al. in their fitting.

**Table 2**
Parameters for Fe–He potentials.

| | Knot coefficient a (eV/nm$^5$) | | Knot point $r$ (nm) | |
|---|---|---|---|---|
| | FeHepot1 | FeHepot2 | | |
| $a_1$ | 2.3177715709828624E−007 | −3.105337419990865E−005 | $r_1$ | 0.2750000 |
| $a_2$ | 2.806803155751341E−005 | 7.664514354111438E−005 | $r_2$ | 0.2928571 |
| $a_3$ | −0.2386549469151253E−005 | −2.063477063257156E−005 | $r_3$ | 0.3107143 |
| $a_4$ | −3.274515978387913E−005 | −4.394916041242475E−005 | $r_4$ | 0.3285714 |
| $a_5$ | 1.589309516491369E−005 | 2.500122908686489E−005 | $r_5$ | 0.3464286 |
| $a_6$ | 8.5836486955798144E−007 | 8.9898217037701151E−007 | $r_6$ | 0.3642857 |
| $a_7$ | −6.8846480862861696E−008 | −0.1297650950021615E−005 | $r_7$ | 0.3821429 |
| $a_8$ | −3.2823533623409129E−007 | −1.2397886870242527E−007 | $r_8$ | 0.4000000 |

**Table 3**
Data list for short range from $R_1$ to $R_2$.

| $r$ (nm) | $f$ (eV) | d$f$/d$r$ (eV/nm) | d$^2f$/d$r^2$ (eV/nm$^2$) |
|---|---|---|---|
| *FeHepot1: $R_1$ = 0.090 nm and $R_2$ = 0.10 nm* | | | |
| 0.090000000 | 12.3556340 | −7.565103700 | 3.8984144100 |
| 0.090500000 | 12.0316366 | −7.293616260 | 3.7414225537 |
| 0.091000000 | 11.7039121 | −7.019115283 | 3.5833796300 |
| 0.091500000 | 11.3724842 | −6.741582753 | 3.4236028512 |
| 0.092000000 | 11.0373349 | −6.461003992 | 3.2620838400 |
| 0.092500000 | 10.6984461 | −6.177364324 | 3.0988142187 |
| 0.093000000 | 10.3557997 | −5.890649070 | 2.9337856100 |
| 0.093500000 | 10.0093778 | −5.600843555 | 2.7669896362 |
| 0.094000000 | 9.65916218 | −5.307933102 | 2.5984179200 |
| 0.094500000 | 9.30513489 | −5.011903032 | 2.4280620837 |
| 0.095000000 | 8.94727785 | −4.712738670 | 2.2559137500 |
| 0.095500000 | 8.58557301 | −4.410425338 | 2.0819645413 |
| 0.096000000 | 8.22000232 | −4.104948359 | 1.9062060800 |
| 0.096500000 | 7.85054773 | −3.796293056 | 1.7286299887 |
| 0.097000000 | 7.47719119 | −3.484444753 | 1.5492278900 |
| 0.097500000 | 7.09991464 | −3.169388771 | 1.3679914063 |
| 0.098000000 | 6.71870003 | −2.851110435 | 1.1849121600 |
| 0.098500000 | 6.33352931 | −2.529595067 | 0.9999817737 |
| 0.099000000 | 5.94438444 | −2.204827989 | 0.8131918700 |
| 0.099500000 | 5.55124735 | −1.876794526 | 0.6245340713 |
| 0.100000000 | 5.15410000 | −1.545480000 | 0.4340000000 |
| *FeHepot2: $R_1$ = 0.096 nm and $R_2$ = 0.10 nm* | | | |
| 0.096000000 | 8.44670300 | −5.527416200 | 2.9112068300 |
| 0.096500000 | 8.17323100 | −5.383065200 | 2.8507379300 |
| 0.097000000 | 7.90691700 | −5.241737700 | 2.7902690200 |
| 0.097500000 | 7.64760800 | −5.103433600 | 2.7298001200 |
| 0.098000000 | 7.36158373 | −4.458324569 | 2.2878111663 |
| 0.098500000 | 7.07247959 | −3.806574405 | 1.8412914077 |
| 0.099000000 | 6.78028126 | −3.148152703 | 1.3902201161 |
| 0.099500000 | 6.48497444 | −2.483029069 | 0.9345765825 |
| 0.100000000 | 6.18654483 | −1.811173106 | 0.4743400982 |

the short range from 0 to $R_1$, the Fe–He dimer data is used [10]. It is found that these potentials are able to be reasonably well fitted to the selected materials data base. The results are listed in Table 1. The substitutional, octahedral and tetrahedral formation energies and migration energy are very close to *ab initio* data [8]. Binding energies for He to He and $He_2$ cluster calculated with FeHepot1 and FeHepot2 are also improved when compared to other published potentials. The actual atomic configurations of $He_2$ and $He_3$ after relaxation with these two potentials are slightly different, where the configuration produced by FeHepot2 is most close to DFT structures [19].

The binding energies of $He_{int}$ to a $He_nV_m$ cluster are also calculated to compare with DFT results [8,19]. All these results are shown in Fig. 1, where it can be seen that the binding energy for $He_nV$ calculated from these two potentials have the similar trend as DFT, but lower by ~0.2 to 0.4 eV. The binding energy for He to $He_nV_m$ ($m > 1$) is close to the DFT results but with differences which originate from the differences between the final lowest states predicted by DFT and these two empirical potentials. As already discussed the migration energy of the tetrahedral He interstitial was

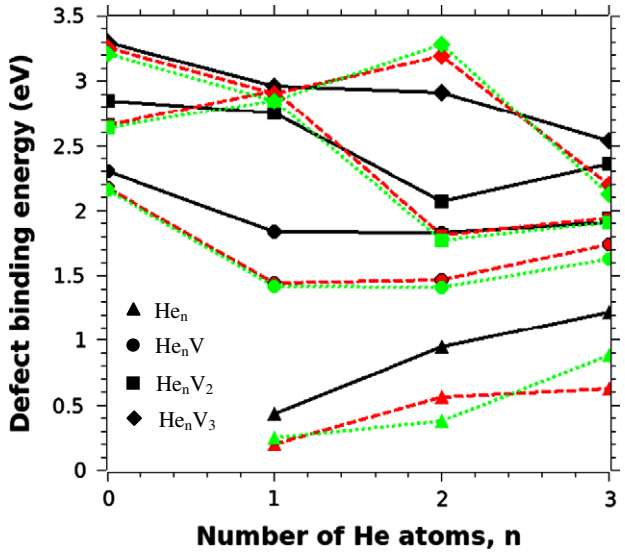


**Fig. 1.** Binding energy of a $He_{int}$ atom to a $He_nV_m$ cluster. The black lines are results from DFT calculations [19]. The green dot lines and red dash lines are results calculated with FeHepot1 and FeHepot2, respectively. (For interpretation of the references to colour in this figure legend, the reader is referred to the web version of this article.)

also fitted using the NEB method. By doing this it became difficult to also fit well to the DFT binding energies of the $He_2$ and $He_3$ clusters. Indeed by removing this migration energy from the materials database, the $He_2$ and $He_3$ formation energies could be well reproduced. The fitted parameters for these two potentials (which includes a good fitted value for the migration energy) are listed in Table 2. The properties shown in Table 1 and Fig. 1 shows that the new potentials can well describe the single He and He-defect cluster binding energy trends in bulk bcc iron. In real materials, most reactions occur in polycrystals with grain boundaries. Therefore in what fallows, we consider the situation of a symmetrical grain boundary, to show some possible applications of new potential in the presence of planar-type defects.

## 4. Applications

The new potentials are used to simulate single He and $He_2$ cluster in $\Sigma3(1\,1\,2)$ grain boundary plane. Only sites in the grain boundary plane are considered for helium atoms and no off-plane sites for $He_2$ are included for search of the most stable configuration. This $\Sigma3(1\,1\,2)$ boundary has well defined tetrahedral and octahedral interstitial positions and a small free volume content. The structures of $\Sigma3(1\,1\,2)$ are shown in Fig. 2 where the local grain boundary plane is (1 1 2). There are several different positions for He as an interstitial atom in this grain boundary plane

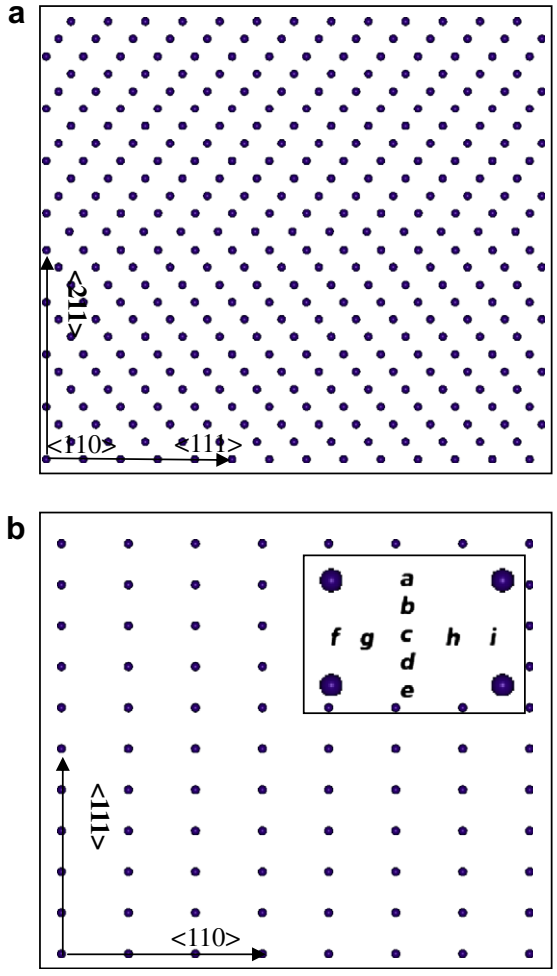


**Fig. 2.** Atomic structures of the Σ3(1 1 2) grain boundary. The directions are also shown, where (a) is the symmetrical grain boundary structure and (b) shows the structure of grain boundary plane. The unit cell of Fe in the grain boundary plane and the possible sites for He atom (*a*–*i*) are shown.

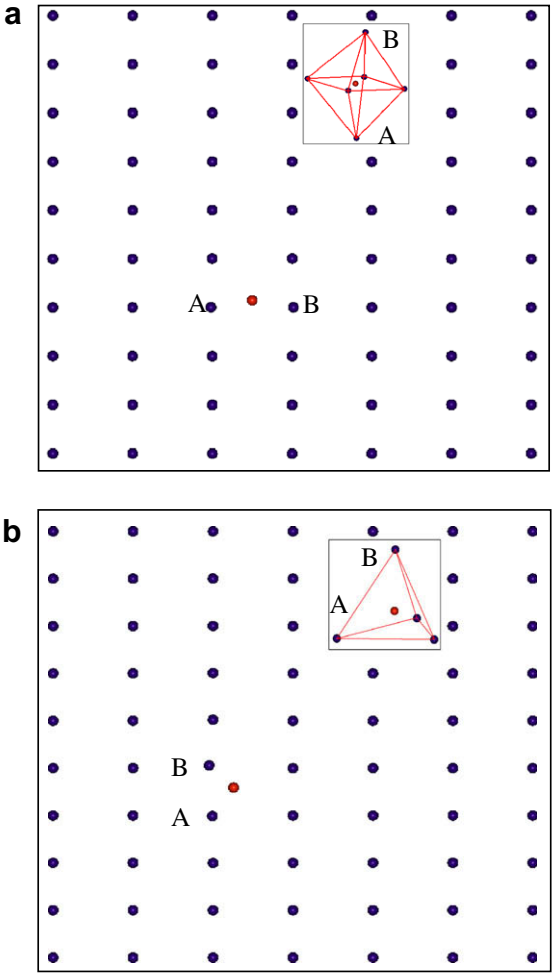


**Fig. 3.** Single He in the Σ3(1 1 2) grain boundary plane. The direction is the same as Fig. 2b. The 3D local structure around the He atom is also shown. Two Fe atoms A and B in the grain boundary plane are indicated in 3D structure. The red and dark points are He and Fe atoms, respectively. (a) Shows the results calculated with Juslin and Nordlund potential; (b) is result calculated with FeHepot1 and FeHepot2. (For interpretation of the references to colour in this figure legend, the reader is referred to the web version of this article.)

as shown in Fig. 2b. In Fig. 2b, site *d* is an octahedral position but site *b* is not because of symmetry reduction due to the grain boundary. Sites *g* and *h* are tetrahedral positions. Site *c* has the biggest free volume. Therefore, several different environments can be chosen by the He atom. The structures are relaxed with the FeHepot1, FeHepot2 and Juslin and Nordlund potentials in order to compare these three different potentials. After relaxations with MD at 0 K with the Juslin and Nordlund Fe–He potential, the most stable position for single He was found to be at site *d*, that is the octahedral interstitial position as shown in Fig. 3a. The results from FeHepot1 and FeHepot2 are similar but differ from results obtained with the Juslin and Nordlund potential. The most stable position for a single He is the *g* or *h* site: the tetrahedral interstitial position shown in Fig. 3b. The local structure of a He atom in grain boundary plane is shown in 3D by connecting bonds between Fe around He atom as indicated in Fig. 3. In Fig. 3a, the normal directions of two perpendicular planes of the octahedral are ⟨1 1 0⟩ and ⟨1 1 2⟩, respectively. In Fig. 3b, the two perpendicular edges of octahedral are parallel to ⟨1 1 1⟩ and ⟨1 1 2⟩ directions, respectively. Two Fe atoms in the grain boundary close to the He atom are also shown to indicate the local relative position of He. The formation energies calculated with these three potentials for single He in Σ3(1 1 2) grain boundary are: 4.03 eV (Juslin and Nordlund potential), 4.01 eV (FeHepot1) and 3.93 eV (FeHepot2). Here, the formation energy of He in symmetrical grain boundary plane is defined as:

$$E_f(\mathrm{He}) = E_{tot}(GB\_\mathrm{He}) - E_{tot}(GB) - E_{\mathrm{He}} \quad (4)$$

where $E_{tot}(GB\_\mathrm{He})$ and $E_{tot}(GB)$ are the total energy of the system with and without He in grain boundary plane, respectively. Based on these formation energies, the binding energy of He to the grain boundary can be calculated as 0.36 eV (Juslin and Nordlund), 0.40 eV (FeHepot1) and 0.51 eV (FeHepot2), which means the helium atoms would be bound to this symmetrical grain boundary. Different initial stable positions (with respect to the *GB*) can result in different He cluster configurations, and depending on the diffusion process in the grain boundary plane, influence the clustering and growing models.

For two He atoms in the Σ3(1 1 2) grain boundary, the most stable configurations calculated with these three potentials are shown in Fig. 4. The results calculated with the Juslin and Nordlund potential are shown in Fig. 4a. The two He atoms occupy two closest octahedral interstitial positions. In Fig. 4b, results calculated with FeHepot1 and FeHepot2 are shown. The two closest octahedrals and tetrahedrals shown in Fig. 4a and b, respectively, have the similar orientations as shown in Fig. 3, as explained above. The two closest tetrahedral interstitial positions are the most stable sites for the He atoms. The local structures around two He atoms are

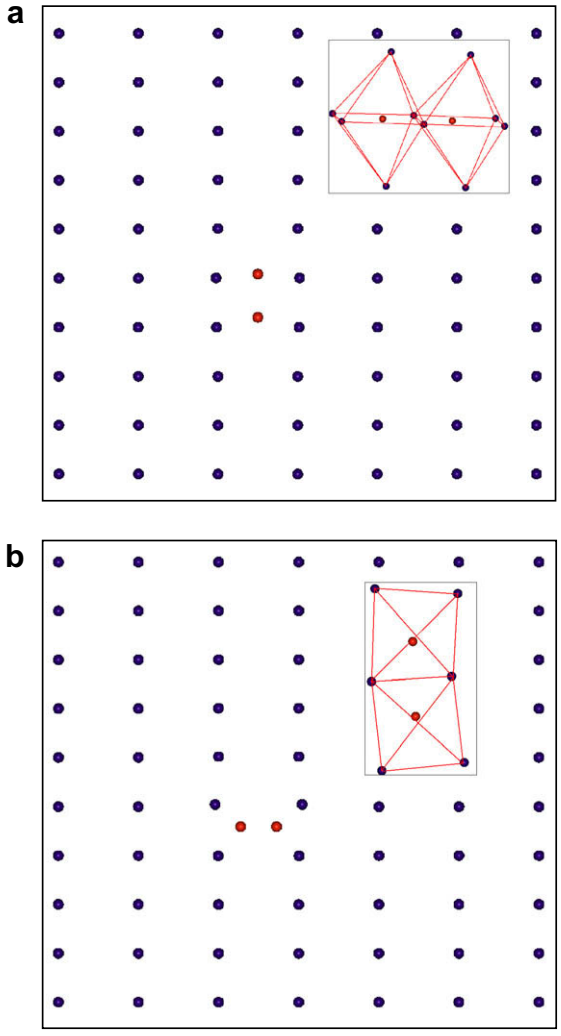


**Fig. 4.** Two He atoms in the Σ3(1 1 2) grain boundary plane. The direction is same as Figs. 2b and 3. The red and dark particles are He and Fe atoms, respectively. (a) Is the results calculated with Juslin and Nordlund potential; (b) is result calculated with FeHepot1 and FeHepot2. (For interpretation of the references to colour in this figure legend, the reader is referred to the web version of this article.)

also shown in 3D and indicated in Fig. 4. The binding energy for the $He_2$ cluster in the Σ3(1 1 2) grain boundary is defined as:

$$E_b(\mathrm{He{-}He}) = E_f(\mathrm{He}) + E_f(\mathrm{He}) - E_f(\mathrm{He_2}) \quad (5)$$

where $E_f(\mathrm{He}_i)$ is formation energy of $\mathrm{He}_i$ cluster in grain boundary plane and calculated with Eq. (4). The results of binding energies calculated with these three potentials are: 0.16 eV (Juslin and Nordlund potential), 0.25 eV (FeHepot1) and 0.18 eV (FeHepot2). Compared with $He_2$ in perfect single crystal, Juslin and Nordlund potential shows increase of $He_2$ binding energy and the new pair potentials, FeHepot1 and FeHepot2, indicate a slightly decrease of $He_2$ binding energy. Thus for this grain boundary, the currently developed potentials (FeHepot1 and FeHepot2) show the tetrahedral geometry as the most stable He interstitial structure, as it is also the case in a perfect crystal for this potential. On the other hand, the Juslin and Nordlund potential suggests the octahedral geometry as the ground state structure in the grain boundary, which differs from the geometry that the same potential gives in the single crystal case, which is the tetrahedral interstitial position. The new potentials show that He atoms prefer to bind with the grain boundary but the binding energy of $He_2$ in the grain boundary is slightly decreased. To determine which potential has the most accurate prediction, *ab initio* work on this particular grain boundary should be done.

## 5. Conclusion

We constructed new Fe–He pair potentials based on recent magnetic Fe potentials and *ab initio* results obtained for the $He_n$ cluster binding energy. The migration energy of tetrahedral He has been included in the fitting. The properties calculated with these two new potentials are reproducing well the *ab inito* values. The applications of these two potentials in the bi-crystal system gave different results to those obtained for the Juslin and Nordlund potential. The tetrahedral interstitial position is the most stable, and the two close tetrahedral interaction positions are the favored sites for $He_2$ in the Σ3(1 1 2) grain boundary. These results are different from the Juslin and Nordlund potential results. The positive binding energy of He to this grain boundary shows He atoms prefer to bind to the grain boundary but the binding energy of $He_2$ in grain boundary plane is slightly lower than the value in the single crystal system. Further work should be done to clarify which potential provides a more accurate result of phenomena occurring in the grain boundary.

## Acknowledgments

The authors would like to acknowledge C.C.Fu (CEA/Saclay) for providing *ab initio* data during the fitting of new potentials and P. M. Derlet (PSI, Switzerland) for very useful discussion and correcting the paper.

## References

[1] H. Ullmaier, W. Schilling, International Atomic Energy Agency, Vienna, 1980.
[2] S.E. Donnelly, J.H. Evans, Fundamental Aspects of Inert Gases in Solids, Plenum, New York, 1991.
[3] T. Ishizaki, Q. Xu, T. Yoshiie, S. Nagata, T. Troev, J. Nucl. Mater. 307–311 (2002) 961.
[4] H. Trinkaus, B.N. Singh, J. Nucl. Mater. 323 (2003) 229.
[5] [a] G. Lucas, R. Schäublin, J. Phys.: Condens. Mater. 20 (2008) 415203; [b] L. Yang, X.T. Zu, H.Y. Xiao, F. Gao, H.L. Heinisch, R.J. Kurtz, K.Z. Liu, Appl. Phys. Lett. 88 (2006) 091915.
[6] R.A. Johnson, W.D. Wilson, in: P.C. Gehlen, J.R. Beeler, R.I. Jaffee (Eds.), Proc. Int. Conf. Interatomic Potentials and Simulation of Lattice Defects, Plenum Press, New York, 1972.
[7] K. Morishita, B.D. Wirth, T. Diaz de la Rubia, A. Kimura, in: Proc. 4th Pacific Rim Int. Conf. on Advanced Materials and Processing (PRICM4), The Japan Institute of Metals, 2001, pp. 1383–1386.
[8] Chu-Chun Fu, F. Willaime, Phys. Rev. B 72 (2005) 064117.
[9] T. Seletskaia, Yu N. Osetskiy, R.E. Stoller, G.M. Stocks, J. Nucl. Mater. 367–370 (2007) 355–360.
[10] N. Juslin, K. Nordlund, J. Nucl. Mater. 382 (2008) 143–146.
[11] He-dpa Workshop in Paul Scherrer Institute (PSI), 2009.
[12] Chu-Chun Fu, F. Willaime, P. Ordejon, Phys. Rev. Lett. 92 (2004) 175503.
[13] [a] S.L. Dudarev, P.M. Derlert, J. Phys – Condens. Mater. 17 (2005) 1; [b] P.M. Derlet, S.L. Dudarev, Prog. Mater. Sci. 52 (2–3) (2007) 299–318.
[14] S. Chiesa, P.M. Derlet, S.L. Dudarev, Phys. Rev. B 79 (2009) 214109.
[15] D.E. Beck, Mol. Phys. 14 (1968) 311.
[16] B. Delley, J. Chem. Phys. 92 (1990) 508.
[17] Dmol is a trademark of AccelRys. Inc. It is a modeling program using DFT to simulate chemical process and predict the properties of materials.
[18] T. Seletskaia, Yu N. Osetskiy, R.E. Stoller, G.M. Stocks, Phys. Rev. Lett. 94 (2005) 046403.
[19] Chu-Chun Fu, F. Willaime, J. Nucl. Mater. 367–370 (2007) 244–250.
[20] Dan Wei, Solid State Physics, first ed., Cengage Learning Asia, 2008 (March 31).
[21] K. Morishita, R. Sugano, B.D. Wirth, J. Nucl. Mater. 323 (2003) 243.
[22] D.J. Hepburn, G.J. Ackland, Phys. Rev. B 78 (2008) 165115.
[23] G. Henkelman, B.P. Uberuaga, H. Jónsson, J. Chem. Phys. 113 (2000) 9901.